Journal of Theoretical Biology 402 (2016) 144–157

Contents lists available at ScienceDirect

Journal of Theoretical Biology

journal homepage: www.elsevier.com/locate/yjtbi

Modeling the diversion of primary carbon flux into secondary metabolism under variable nitrate and light/dark conditions

Romain Larbat [a,b,*], Christophe Robin [a,b], Cathrine Lillo [c], Tormod Drengstig [d], Peter Ruoff [c,**]

[a] INRA UMR 1121, Agronomie & Environnement Nancy-Colmar, TSA 40602, 54518 Vandoeuvre Cedex, France
[b] Université de Lorraine UMR 1121, Agronomie & Environnement Nancy-Colmar, TSA 40602, 54518 Vandoeuvre Cedex, France
[c] Centre for Organelle Research, University of Stavanger, Stavanger Innovation Park, Måltidets Hus, 4021 Stavanger, Norway
[d] Department of Computer Science and Electrical Engineering, University of Stavanger, 4036 Stavanger, Norway

HIGHLIGHTS

- A model connecting primary and secondary carbon metabolism by sucrose homeostasis.
- Experimental starch levels at different light–dark cycles are described.
- Suggesting mechanisms of day length measurement with respect to starch regulation.
- Describing starch profile kinetics when changing to short or long day lengths.
- PAP1 and sucrose regulation based on the experimental autocatalytic formation of TT8.

ARTICLE INFO

Article history:
Received 22 February 2016
Received in revised form
2 May 2016
Accepted 5 May 2016
Available online 6 May 2016

Keywords:
Sucrose homeostasis
Phenolic pathway
Starch
Negative feedback
Integral control
Nitrate availability
Day-length measurement

ABSTRACT

In plants, the partitioning of carbon resources between growth and defense is detrimental for their development. From a metabolic viewpoint, growth is mainly related to primary metabolism including protein, amino acid and lipid synthesis, whereas defense is based notably on the biosynthesis of a myriad of secondary metabolites. Environmental factors, such as nitrate fertilization, impact the partitioning of carbon resources between growth and defense. Indeed, experimental data showed that a shortage in the nitrate fertilization resulted in a reduction of the plant growth, whereas some secondary metabolites involved in plant defense, such as phenolic compounds, accumulated. Interestingly, sucrose, a key molecule involved in the transport and partitioning of carbon resources, appeared to be under homeostatic control. Based on the inflow/outflow properties of sucrose homeostatic regulation we propose a global model on how the diversion of the primary carbon flux into the secondary phenolic pathways occurs at low nitrate concentrations. The model can account for the accumulation of starch during the light phase and the sucrose remobilization by starch degradation during the night. Day-length sensing mechanisms for variable light–dark regimes are discussed, showing that growth is proportional to the length of the light phase. The model can describe the complete starch consumption during the night for plants adapted to a certain light/dark regime when grown on sufficient nitrate and can account for an increased accumulation of starch observed under nitrate limitation.

1. Introduction

Plants live in a world of competition; they need resources (light, nutrients, water) to grow over neighbors, and need to defend against herbivores and parasites. Plant growth relies on processes of cell division, cell elongation and maintenance within the cell which involve mainly the primary metabolism. Plant defense, on the other hand, relies notably on the development of differentiated structures (such as trichomes and spines) and on the synthesis of secondary metabolites, such as phenolics, alkaloids, carotenoids and other products. Plant growth and defense share a common carbon (C) source, i.e., photosynthates (Loomis, 1932; McKey, 1974; Bryant et al., 1983). The defense costs on plant fitness, the trade-off result between growth and defense, are of great

* Corresponding author at: INRA UMR 1121, Agronomie & Environnement Nancy-Colmar, TSA 40602, 54518 Vandoeuvre Cedex, France.
** Corresponding author.
E-mail addresses: romain.larbat@univ-lorraine.fr (R. Larbat), peter.ruoff@uis.no (P. Ruoff).

http://dx.doi.org/10.1016/j.jtbi.2016.05.008
0022-5193/

interest for plant ecologists studying plant–pathogens relationships (Züst et al., 2011; Mooney et al., 2010). This trade-off between growth and defense is also an important aspect for agronomists. Understanding the relationships between growth and defense will help to develop new agricultural practices to maintain plant defense while still keeping a high crop production (ecological intensification concept; for review, see Doré et al., 2011).

During the last decades, several hypotheses have been suggested to describe the distribution of resources to growth and defense with respect to the availability of resources (for review, see Stamp, 2003). Among them, the Growth Differentiation Balance Hypothesis (GDBH) is considered as the most mature one (Loomis, 1932; Herms and Mattson, 1992; Stamp, 2004). The GDBH states that the growth takes priority over the defense and distinguishes three domains of resource availability: (i) a severe resource deficiency where C assimilation, the relative growth rate and the relative rate of secondary metabolism are positively correlated to the limiting resource; (ii) a moderate resource limitation where C assimilation is no longer limited, while the relative growth rate still is. In this domain, most of the assimilated C that is not used for plant growth is diverted to the secondary metabolism. It results in a negative correlation between the relative rate of secondary metabolism and the relative growth rate; (iii) in the third domain, the relative growth rate is no longer limited and requires the major part of the assimilated C at the expense of the secondary metabolism whose rate is maintained at a low level (Herms and Mattson, 1992; Le Bot et al., 2009).

Although the GDBH considers any plant resources (except light, which influences C assimilation more than growth) a large body of the literature aiming to test this hypothesis has been focused on the nitrate (N) availability and led to controversial conclusions. On the one hand, as expected by the hypothesis, N limited plants generally exhibit a slow growth rate and an increase in soluble phenolics, a large family of C-rich secondary metabolites involved in plant defense (Le Bot et al., 2009; Larbat et al., 2012; Royer et al., 2013; Stewart et al., 2001; Nguyen and Niemeyer, 2008; Glynn et al., 2007). On the other hand, the content of other C-rich secondary metabolites like terpenes, tannins and also lignin, the main compound of the plant structure and cell wall reinforcement, do not follow the predictions of the GDBH (Massad et al., 2012; Koricheva et al., 1998; Royer et al., 2013). These examples indicate that global conceptual models could not properly describe the response diversity of the secondary metabolism to resources availability. They highlight the need to develop complementary models taking into account knowledge on key metabolic pools together with their relationships and regulations. The aim of our present work was to provide such a model on the impact of N availability on the C flux toward the primary metabolism and the phenolic pathway taken as representative of the secondary metabolism.

Nitrogen is a major nutrient for plants. It is an essential constituent of amino acids and proteins, nucleic acids, co-factors and the photosynthetic apparatus (Chlorophylls, Rubisco), making it a key element to sustain plant growth (Marschner, 2012). With the exception of legumes, nitrogen is assimilated by plants through inorganic forms, the major one being nitrate (N) in aerobic soils (Xu et al., 2012). N and derived metabolites are also signaling molecules up-regulating genes involved in N assimilation, photosynthesis and primary metabolism (amino acid synthesis, pentose phosphate pathway) and repressing the expression of several genes in the phenylpropanoid pathway (Vidal and Gutierrez, 2008; Fritz et al., 2006). The effect of N limitation on the increase in the phenolic content mentioned above is correlated with an up-regulation of the expression of the phenylpropanoid specific genes (Fritz et al., 2006; Lillo et al., 2008). In addition, a limitation in the N fertilization triggers also a variety of responses in the carbohydrate and primary metabolisms at the metabolic level that is at least partly due to large regulations at the transcriptome level (Scheible et al., 2004; Fritz et al., 2006). Indeed, the main features observed in plant leaves are a decrease in the concentrations of individual amino acids (Fritz et al., 2006), proteins (Kingston-Smith et al., 2005) and organic (citric and malic) acids (Le Bot et al., 2009; Royer et al., 2013), an increase in hexoses (Le Bot et al., 2009), whereas the concentration of sucrose is maintained nearly constant or is less affected (Le Bot et al., 2009; Fritz et al., 2006; Pretorius et al., 1999; Abro et al., 2013; Geiger et al., 1999).

Sucrose represents a pivotal molecule for plant metabolism. It constitutes the major form of C transport between tissues and organs and is also a signaling molecule regulating large aspects of the cell metabolism (for review, Wind et al., 2010). During the day, sucrose is synthesized in the cytosol from the Calvin cycle products (triose phosphates) and, during the night, from the breakdown of accumulated starch (Stitt and Zeeman, 2012; Huber et al., 1992). Sucrose biosynthesis is highly regulated notably through a feed-forward regulation on the fructose-1,6-phosphatase (F1,6Pase) and a feed-back regulation on the sucrose phosphate synthase (SPS) and the F1,6Pase (Huber et al., 1992). The role of sucrose as signaling molecule is less documented than glucose. However, sucrose was firmly proved to repress the expression of plastocyanin, a photosynthetic gene (Dijkwel et al., 1996) and the transcription factor bZIP11 involved in the regulation of amino acids biosynthesis in Arabidopsis (Hanson et al., 2008). Sucrose also up-regulates the expression of anthocyanin genes (Solfanelli et al., 2006).

The conceptual basis of the model we describe in this paper is to consider the maintenance of the sucrose homeostasis under variable nitrate (N) availability as a determinant of the C partitioning between the primary and the secondary metabolisms. When sufficient N is available to the plant, sucrose is funneled into the primary C metabolism as N activates this pathway (for review, see Vidal and Gutierrez, 2008). Under these conditions, the sucrose homeostasis is maintained by an inflow control mechanism (for mechanistic details see next section), which provides the sufficient C-flux required by the N activated primary C metabolism. At lower and growth limiting N conditions, the primary C-flux is diminished due to the lower activation by N. But, as a consequence of the still unchanged photosynthetic activity, sucrose is still formed from trioses-P. To keep sucrose at a constant homeostatic level, the excess of produced sucrose, which cannot enter the primary C-flux, is now diverted into the secondary C metabolism, by the use of an outflow mechanism (for mechanistic details see next section). The major metabolic pathway served is thus the soluble phenolics pathway. Besides the diversion of primary C-flux into the phenolic pathway the model can also account for the increased accumulation of starch under N limiting condition and the accumulation and remobilization of starch into sucrose under diurnal and variable light–dark conditions.

2. Modeling sucrose homeostasis

An essential property of all cells and organisms is their homeostatic regulation of a wide range of components. The term ‘homeostasis’ was introduced by Cannon while showing that many compounds and physiological parameters in cells and organisms are kept within certain and often narrow limits (Cannon, 1929).

In biochemical systems, robust homeostasis can be achieved by combining a negative feedback with integral control (Yi et al., 2000). While robust regulation by integral control is well established in control engineering (Wilkie et al., 2002), kinetic principles leading to integral control in biochemical systems were only recently found (Ni et al., 2009; Huang et al., 2012; Drengstig et al., 2012a,b; Thorsen et al., 2013). These studies showed that

homeostatic controller motifs fall into two classes termed as inflow and outflow controllers (Drengstig et al., 2012a). Inflow controllers provide homeostasis by adding the controlled variable to the system by a compensatory flux from an internal or external source. Inflow controllers compensate for outflow perturbations, which act on the controlled variable. Outflow controllers work oppositely. They remove the excess of the controlled variable (due to inflow perturbations) by excreting or moving it to an internal store.

In the following, we show how the combination of inflow and outflow controllers can describe sucrose homeostasis in plant and the associated daily buildup and degradation of starch at different light–dark regimes. When N becomes limiting for the plant growth the combined controllers divert the primary C-flux into the secondary metabolism in order to maintain plant sucrose homeostasis.

3. The model

Fig. 1 gives an overview of the model which is defined at the global plant scale. Rate equations and parameter values are listed in the appendices and figure legends, respectively. Sucrose synthesis occurs by two main reaction paths. During the day sucrose is formed by photosynthesis via triose-phosphates (triose-P). Photosynthetic CO_2 assimilation and regulations are well described in the literature. For the sake of simplicity these regulations were not considered here. For details, see Farquhar et al. (1980) and Von Caemmerer and Farquhar (1981). During the night, when there is no photosynthetic activity, sucrose is formed from starch that has been synthesized during the previous day. At sufficiently high N concentrations sucrose is directed into the primary C metabolism, which generates compounds involved in plant growth (notably amino acids and proteins). The secondary C-flux leads to the production of soluble phenolics, which increase in concentration when N availability is limiting for the plant growth (Fritz et al., 2006; Le Bot et al., 2009). Part of the secondary C-flux leads also to the synthesis of lignin, but here no regulation has been demonstrated.

Internal nitrate levels in plant leaves and roots have been found to be under homeostatic control (Miller and Smith, 1992, 2008). In order to account for this here, the uptake of N is described by an inflow-type of controller as done previously (Huang et al., 2012). However, for the sake of simplicity N storage and remobilization, which take also part in the nitrate homeostatic mechanism, are not considered here.

Internal N favors photosynthesis and growth through gene activation (for review, see Vidal and Gutierrez, 2008).This is represented in the model by a N-activation of the triose-P formation and the activation of sucrose entry to the primary C-flux. In the model, the N-activations are described by the activating function

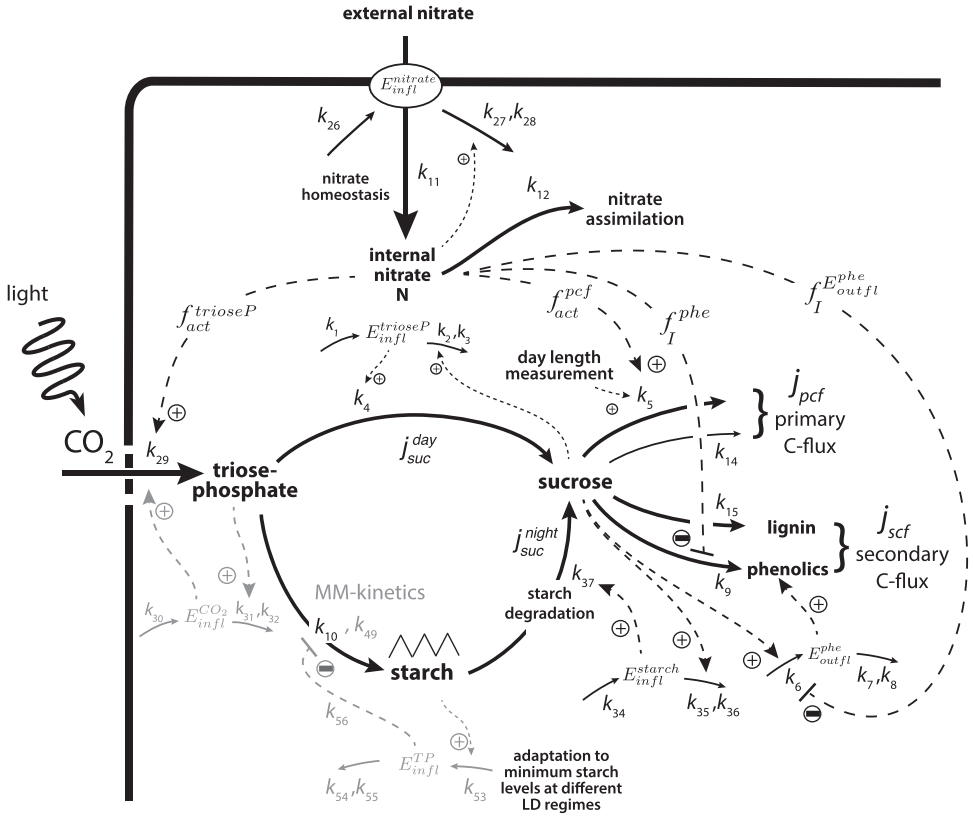

Fig. 1. Plant model for sucrose homeostasis under variable nitrate (N) availability. Grayed sections are successively included. During the day, triose-phosphate formed from the photosynthesis is shared between the synthesis of starch and the synthesis of sucrose. Sucrose is used for the formation of primary carbon (C) compounds as well as secondary compounds (phenolics) and lignin. The demand for sucrose is regulated by at least one inflow controller including SnRK1. In the model, this inflow control is represented by $E_{infl}^{trioseP}$ (see discussion). During the night, sucrose is formed from starch via a remobilization pathway and regulated by inflow controller E_{infl}^{starch}. The adaptation to a minimal starch level at dawn at different light/dark regimes is performed by a starch inflow controller E_{infl}^{TP} (outlined in gray). Because internal N is kept at a homeostatic level, maximum activation of the primary C pathway by $E_{infl}^{trioseP}$ is ensured by sufficient external N concentrations. When external N is getting so low such that the high affinity uptake system of N is not able to maintain internal N homeostasis, the primary C-flux decreases due to a lower N-activation on k_5. Since photosynthesis is less sensitive to N limitation than growth (due to the different activation constants k_{13} and k_{33} in f_{act}^{pcf} and $f_{act}^{trioseP}$, respectively, the N activation on the photosynthetic activity (k_{29}) is still maintained and sucrose is still formed. To avoid a build-up of sucrose and to keep sucrose at a homeostatic level, excess of C is diverted by outflow controller E_{outfl}^{phe} into the phenolic pathway (see discussion).

$$f_{act}^{X} = f_{act,max}^{X}\left(\frac{N}{K_{act}^{X}+N}\right) \quad (1)$$

where N is the concentration of nitrate and K_{act}^{X} is an activation constant. X is a variable, which describes the target of the activation, i.e., either triose-phosphates (triose-P) or the primary C-flux (pcf). When N is high compared to K_{act}^{X}, f_{act}^{X} reaches its maximum value $f_{act,max}^{X}$. Different $f_{act,max}^{X}$ and K_{act}^{X} values are assumed for the activation of the primary C metabolism and triose-P. N exerts also a repressing effect on the phenolic pathway (Fritz et al., 2006), which we have included in the model by inhibitory functions of the form

$$f_{I}^{Y} = f_{I,max}^{Y}\left(\frac{K_{I}^{Y}}{K_{I}^{Y}+N}\right) \quad (2)$$

where Y denotes the target compound of the inhibition.

Remobilization of sucrose from starch is described by an inflow controller E_{infl}^{starch} with its own homeostatic set-point, considering that the plant has a demand for sucrose also during the night. To keep sucrose at a robust homeostatic level, two other control steps are included into the model. When the demand for sucrose is high at light and high N concentrations leading to increased growth rates, the inflow controller $E_{infl}^{trioseP}$ enables the necessary sucrose delivery for the primary C metabolism while maintaining sucrose homeostasis. When N concentrations become growth-limiting (domain ii of the GDBH; see above), the primary C-metabolism is reduced, while photosynthesis is still maintained. Thus, as photosynthesis remains practically unaltered at growth-limiting conditions, sucrose is still produced and will eventually exceed the set-point of the inflow controller $E_{infl}^{trioseP}$. To avoid a build-up of sucrose at low N availability, the excess of produced sucrose is now redirected into the phenolic pathway by outflow controller E_{outfl}^{phe}, which acts concomitantly with the de-repressing effect described by f_{I}^{phe}.

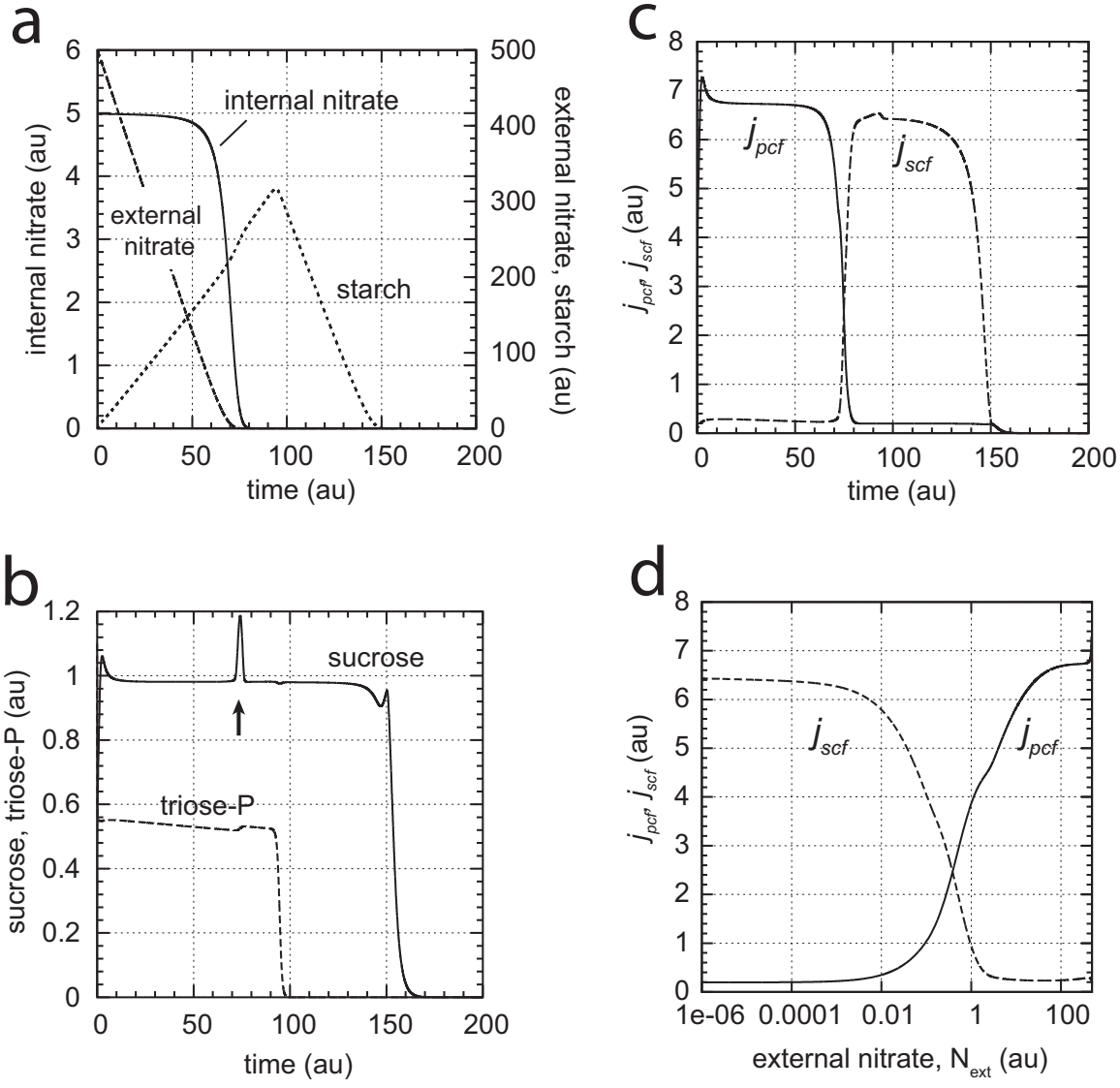

Fig. 2. Sucrose homeostasis and the partitioning from the primary C-flux into the secondary metabolism at low external N (without the grayed sections in Fig. 1). (a) Internal N levels are kept under homeostatic control while external N levels are decreasing. During this period, photosynthesis is maintained and triose-P is transformed into starch and sucrose while sucrose levels remain at their homeostatic level. (b) Sucrose homeostasis (with a set-point of 1). (c) Primary and secondary C-fluxes. When external N concentrations become very low, the internal N concentration decreases, which leads to a decrease in the primary C-flux j_{pcf} and a temporary increase of sucrose (arrow, panel b), but outflow controller E_{outfl}^{phe} increases j_{scf} and maintains sucrose homeostasis. (d) j_{pcf} and j_{scf} levels at different N_{ext}. Rate constant values and initial concentrations (in au): $k_1 = 1.0$, $k_2 = 1.0$, $k_3 = 1.0 \times 10^{-5}$, $k_4 = 1.0$, $k_5 = 8.0$, $k_6 = 10.0$, $k_7 = 9.8$, $k_8 = 1.0 \times 10^{-6}$, $k_9 = 1.0$, $k_{10} = 10.0$, $k_{11} = 0.2$, $k_{12} = 1.5$, $k_{13} = 1.0$, $k_{14} = k_{15} = 0.2$, $k_{16} - k_{25}$ not used, $k_{26} = 0.5$, $k_{27} = 0.1$, $k_{28} = 1.0 \times 10^{-6}$, $k_{29} = 10.1$, $k_{30} = k_{31} = 0.0$, $k_{32} = 1.0 \times 10^{-5}$, $k_{33} = 1.0 \times 10^{-11}$, $k_{34} = 9.8$, $k_{35} = 10.0$, $k_{36} = 1.0 \times 10^{-4}$, $k_{37} = 0.1$, $k_{38} = 0.2$, $k_{39} = 1.0 \times 10^{3}$, $sucr_0 = 2.84$, $E_{infl,0}^{trioseP} = 8.06$, $E_{outfl,0}^{phe} = 1.0 \times 10^{-5}$, $N_0 = 5.00$, $\text{starch}_0 = 0.0$, $N_{ext,0} = 500.0$, $E_{infl}^{nitrate} = 7.5 \times 10^{-2}$, $\text{trioseP}_0 = 1.10$, $E_{infl,0}^{CO_2} = 1.0$ (kept constant), and $E_{infl,0}^{Starch} = 1.0 \times 10^{-4}$.

To get a stable production of starch, the triose-P level was kept constant due to an inflow-type of controller $E_{infl}^{CO_2}$. To describe the experimentally observed starch synthesis and degradation at different light–dark regimes molecular mechanisms to measure the amount of received light by the plant are suggested (see below).

Rate equations were solved numerically by using the FORTRAN subroutine LSODE (Livermore Solver of Ordinary Differential Equations) (Radhakrishnan and Hindmarsh, 1993) and MATLAB/SIMULINK (www.mathworks.com). To make notations simpler, concentrations of compounds are indicated by compound names without square brackets.

4. Sucrose homeostasis and secondary carbon flux induction

To illustrate the dynamic behaviors of the model and the diversion of the primary carbon flux into the phenolic pathway at low external N concentrations, we first consider the situation when different external N concentrations are present. Fig. 2 shows a calculation where the external N concentration successively decreases as N is taken up by the plant. Due to the inflow controller $E_{infl}^{nitrate}$, the internal N concentration is kept approximately constant during its uptake, but decreases rapidly when the external N source becomes exhausted (Fig. 2a). During the uptake of N, the starch content in the cell increases. During this period, sucrose homeostasis is maintained by inflow controller $E_{infl}^{trioseP}$, while the primary C-flux, j_{pcf}, is relatively high compared to the secondary C-flux into the phenolics pathway, j_{scf} (Fig. 2b and c). For the sake of simplicity the set-point of sucrose was defined to 1. When the external and internal N concentrations are getting low, there is a phase when photosynthesis is still operating but the primary C-flux j_{pcf} is decreasing. During this stage, starch is still synthesized and sucrose level temporarily rises (arrow, Fig. 2b). The temporary rise in sucrose level is due to the decrease in the j_{pcf} flux by the diminished internal N activation (via f_{act}^{pcf}, Fig. 1) and

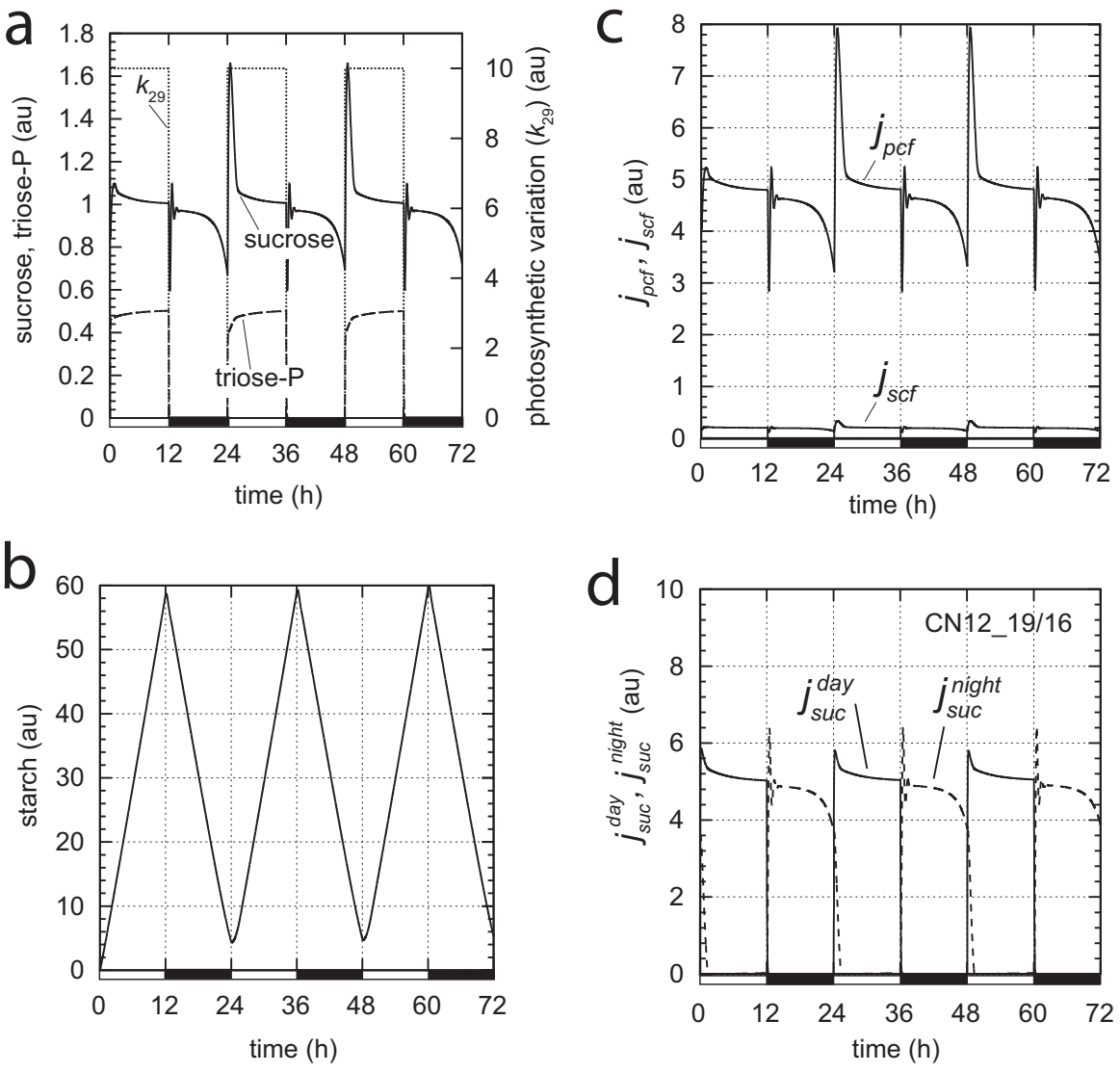

Fig. 3. Model calculation at 12 h/12 h light/dark (LD) changes. At light conditions $k_{29} = 10.1$, while during darkness $k_{29} = 0.0$. The concentration of external nitrate (N_{ext}) is at a relative high level (20.0) and kept constant. (a) Level of sucrose and triose-P during LD changes. The spikes at the LD transitions are due to the sudden change in k_{29} and considered as artefacts. (b) At this relative high value of N_{ext} the primary C-flux, j_{pcf}, is higher than the secondary one, j_{scf}. (c) Starch levels show constant synthesis and degradation rates. Rate constant values and initial concentrations (in au): $k_1 = 1.0$, $k_2 = 1.0$, $k_3 = 1.0 \times 10^{-5}$, $k_4 = 5.0$, $k_5 = 5.5$, $k_6 = 10.0$, $k_7 = 9.8$, $k_8 = 1.0 \times 10^{-6}$, $k_9 = 1.0$, $k_{10} = 10.0$, $k_{11} = 0.2$, $k_{12} = 15.0$, $k_{13} = 1.0$, $k_{14} = k_{15} = 0.2$, $k_{16} - k_{25}$ not used, $k_{26} = 0.5$, $k_{27} = 0.1$, $k_{28} = 1.0 \times 10^{-6}$, $k_{29} = 10.1$, $k_{30} = k_{31} = 0.0$, $k_{32} = 1.0 \times 10^{-5}$, $k_{33} = 1.0 \times 10^{-11}$, $k_{34} = 9.8$, $k_{35} = 10.0$, $k_{36} = 1.0 \times 10^{-4}$, $k_{37} = 0.1$, $k_{38} = 2.0 \times 10^{-2}$, $k_{39} = 1.0 \times 10^{3}$. $\text{sucr}_0 = 0.748$, $E_{infl,0}^{trioseP} = 2.825$, $E_{outfl,0}^{phe} = 9.751 \times 10^{-7}$, $N_0 = 4.998$, $\text{starch}_0 = 6.041$, $N_{ext,0} = 20.0$ (kept constant), $E_{infl,0}^{nitrate} = 18.742$, $\text{trioseP}_0 = 0.0$, $E_{infl,0}^{CO_2} = 1.0$ (kept constant), and $E_{infl,0}^{starch} = 5.950$.

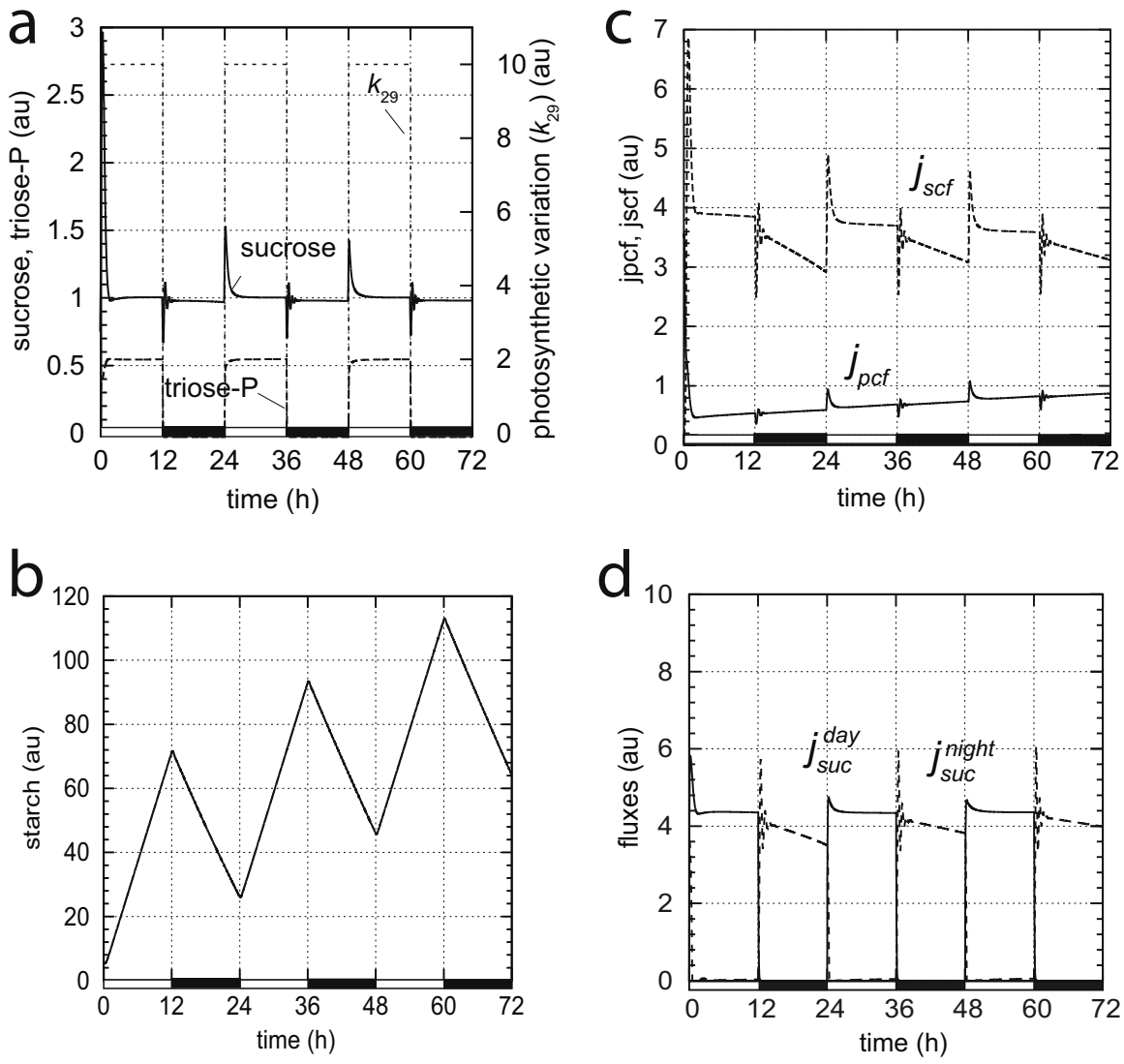

Fig. 4. Rate constants and initial concentrations as in Fig. 3, but at low constant $N_{ext,0} = 2.0 \times 10^{-2}$. (a) Sucrose level is kept at its homeostatic set-point of 1.0. (b) As observed experimentally (Le Bot et al., 2009) starch levels are elevated when external N levels are low. (c) At low N_{ext} concentrations the j_{scf} flux is increased to maintain sucrose homeostasis during light and dark conditions. (d) Sucrose forming flux during light (j_{suc}^{day}) and dark (j_{suc}^{night}) conditions maintaining sucrose homeostasis.

because the outflow controller E_{outfl}^{phe} has not fully established its function. Once the outflow controller E_{outfl}^{phe} has taken control, sucrose is diverted into the phenolic pathway. At this stage, sucrose homeostasis is re-established and j_{scf} is at a high level relative to j_{pcf} (Fig. 2c). When N availability becomes so low that photosynthesis can no longer be maintained, sucrose is synthesized from the starch pool and sucrose homeostasis maintained by outflow controller E_{outfl}^{phe} until all starch is used up (Fig. 2a). Fig. 2d shows how j_{scf} and $jpcf$ levels from Fig. 2c depend on the amount of external N and shows their respective up- and down-regulation when external N levels are getting low.

We tested the model under high (Fig. 3) and low (Fig. 4) external N availabilities for three successive nycthemeral periods. In each simulation the day/night transition was simulated by switching off the constant k_{29}, related to the photosynthesis, which was put back to its initial values at the end of the night period (Fig. 3a). Evolution of triose-P, sucrose, and the starch pool were followed over the three nycthemeral periods. Triose-P quickly reached a plateau during the day and then went to zero during the night, as a consequence of the photosynthesis switch off.

Sucrose concentrations show a transient decrease or increase after respective light to dark (L → D) or dark to light (D → L) transitions (Fig. 3a), which is also seen in experiments (see Fig. 4 in Lu et al., 2005). However, compared with the experimental results the model transient peaks are relatively large, which we consider as a model artefact due to the abrupt changes made in k_{29}.

Starch evolution exhibited, as found by experiments (Smith and Stitt, 2007; Gibon et al., 2004), a typical saw-tooth profile, characterized by a linear accumulation during the day and an almost complete linear degradation during the night (Fig. 3c). At high external N availability, the primary C-flux j_{pcf} was much higher than the secondary C-flux j_{scf} (Fig. 3b). Both fluxes behaved similar to the sucrose evolution, i.e., with an artifactual peak at the start of light period, then maintaining a steady state level during the day and the first part of the night, before decreasing at the end of the night (Fig. 3b). Under limited external N availability, the daily steady state level of triose-P was little affected (Fig. 4a). Sucrose was maintained at its homeostatic set-point as under high N availability, but did not decrease during the second half of the night (Fig. 4a). The secondary C-flux j_{scf} was now clearly higher than j_{pcf}, although the primary C-flux showed an increasing trend (Fig. 4c). Compared to the high N availability, starch evolution was characterized by an increased accumulation during the day and a limited degradation during the night, resulting in starch accumulation day after day (Fig. 4b).

Sucrose-forming fluxes during light (j_{suc}^{day}) and dark (j_{suc}^{day}) conditions maintain sucrose homeostasis (Fig. 4a and d).

5. Starch content during different light–dark regimes

Starch accumulation and mobilization is under circadian regulation (Lu et al., 2005). The rate of starch degradation is set by mechanisms that 'measure' the amount of starch in leaves at the end of the day and anticipate the length of night in order to maintain a constant supply of C through the night (Smith and Stitt, 2007). Arabidopsis plants, which are adapted to different light–dark periods, have been found to regulate their starch content in such a way that at the end of the night period approximately all daily produced starch is utilized (Gibon et al., 2004). The dark circles in Fig. 5a show the starch content of plants which have been adapted to a 6:18 light:dark regime, while the open squares show the starch content in plants adapted to a 12:12 light:dark regime. How plants manage to optimize their starch usage under different light dark conditions is still not well understood and different approaches have been suggested (Feugier and Satake, 2013; Scialdone et al., 2013; Pokhilko et al., 2014; Seaton et al., 2014; Pokhilko and Ebenhöh, 2015; Scialdone and Howard, 2015). In the following we give a brief description of these approaches.

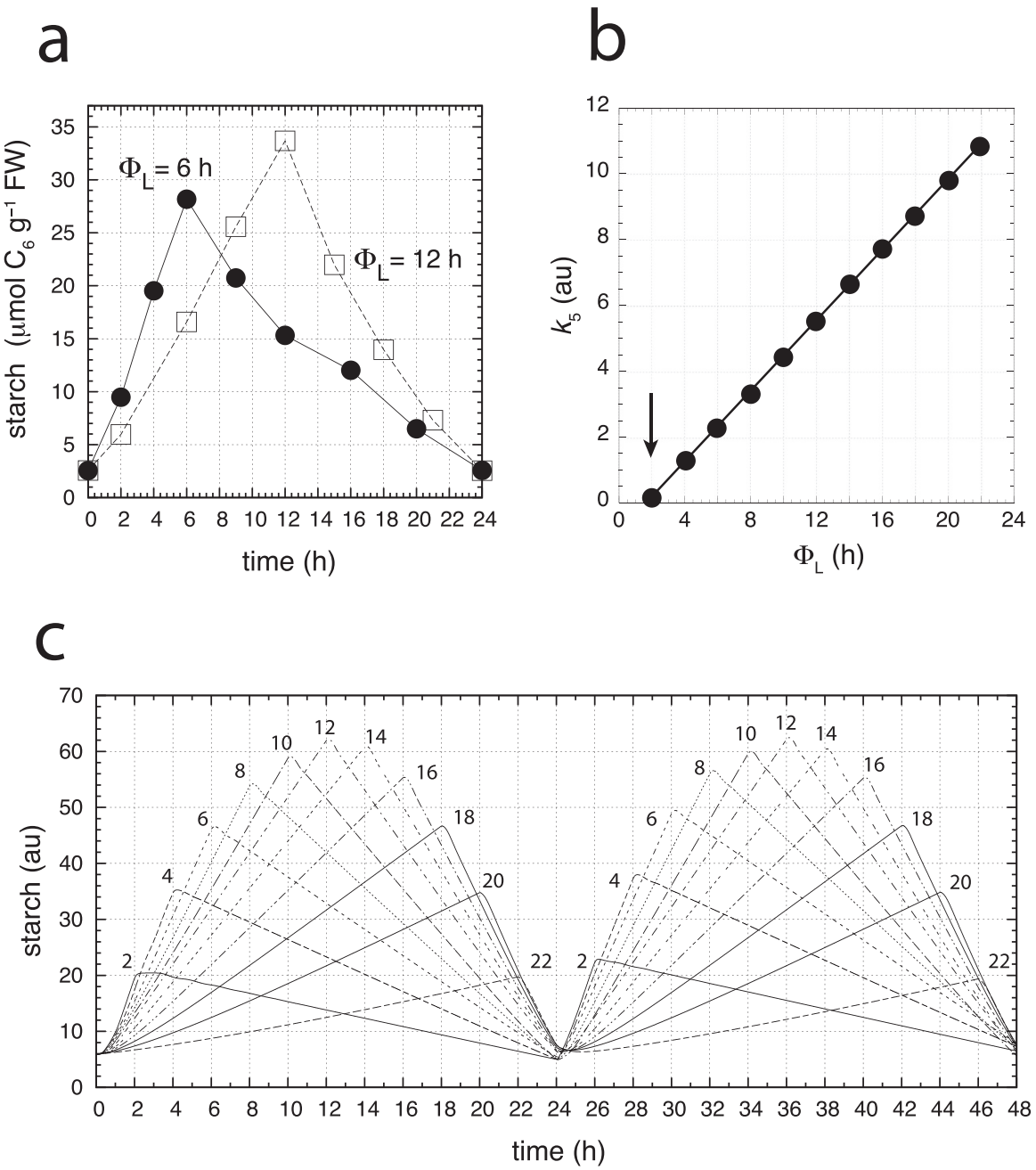

Fig. 5. Starch regulation at different light–dark (LD) cycles. (a) Starch levels in Arabidopsis plants adapted to 6 h/18 h and 12 h/12 h L/D cycles. Φ_L describes the day length. In the LD adapted plants, the production of starch during the day matches precisely its consumption during the following night (Gibon et al., 2004). (b) In order to achieve that the amount of produced starch during the day matches the amount of starch consumed during the next night, the model predicts that k_5, i.e., part of the primary C-flux, needs to be proportional to the day length Φ_L. The arrow indicates the plant's compensation point, i.e., a minimum day length is required to maintain the system even when no starch is produced. (c) Behavior of starch levels at different day lengths Φ_L when k_5 follows the relationship in panel (b). The other rate constants and initial concentrations are as in Fig. 3.

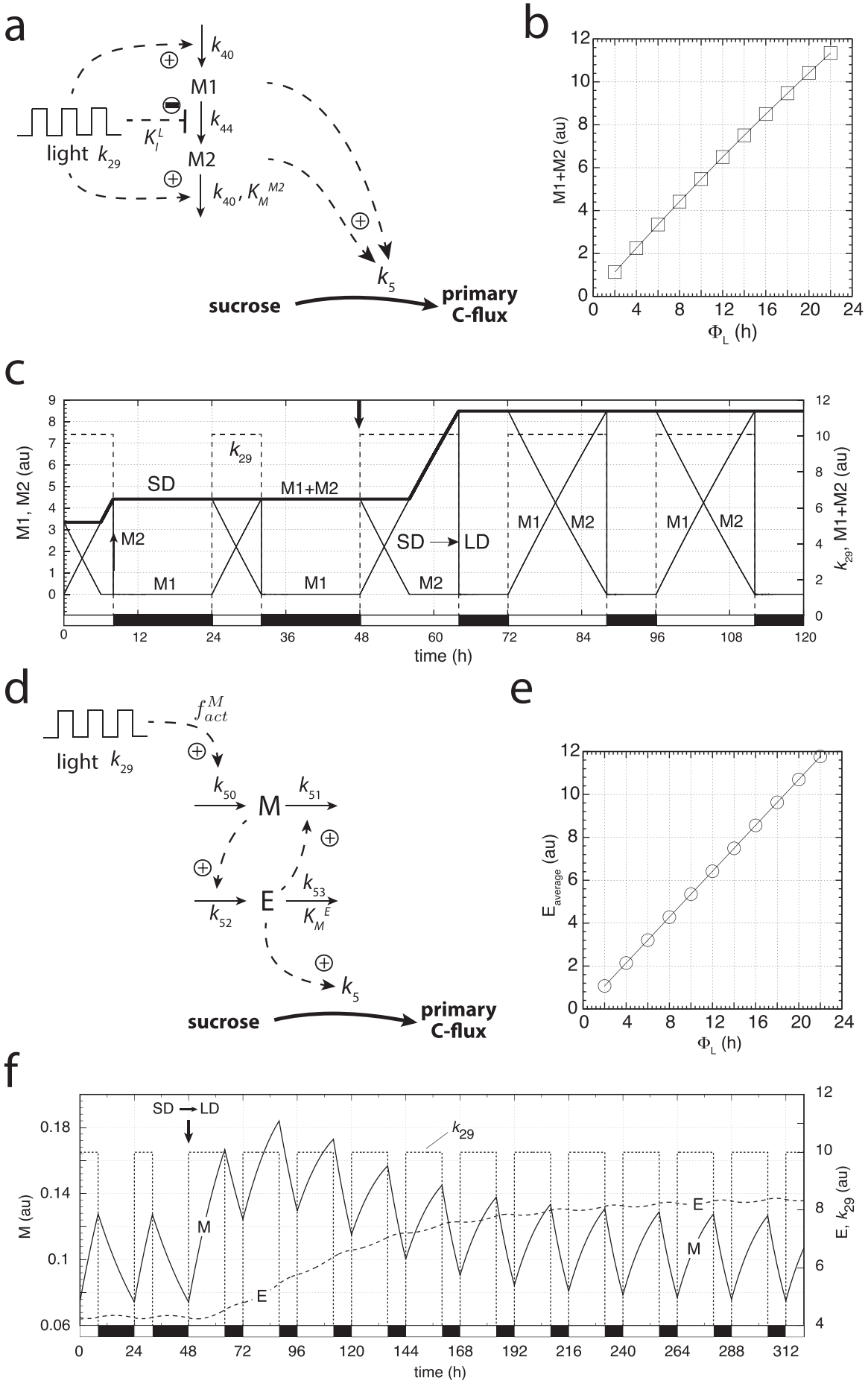
a
k_{40}
M1
k_{44}
K_I^L
light k_{29}
M2
k_{40}, K_M^{M2}
k_5
sucrose
primary C-flux
b
M1+M2 (au)
Φ_L (h)
c
M1, M2 (au)
k_{29}, M1+M2 (au)
SD
M1+M2
k_{29}
M2
M1
M1
M2
SD → LD
M1
M2
M1
M2
time (h)
d
f_{act}^M
light k_{29}
k_{50}
M
k_{51}
k_{52}
E
k_{53}
K_M^E
k_5
sucrose
primary C-flux
e
$E_{average}$ (au)
Φ_L (h)
f
SD → LD
k_{29}
M (au)
E, k_{29} (au)
M
E
E
M
time (h)

In the work by Feugier and Satake (2013) the optimization of starch usage is accomplished by a feedback relationship between the circadian clock affecting the sucrose/starch metabolism which feeds back to the clock and induces phase shifts. Their modeling results show that almost all features of experimental starch profiles can be explained by their feedback hypothesis. Scialdone et al. (2013) and Scialdone and Howard (2015) suggested a mechanism which can be associated with an arithmetic division calculation that anticipates dawn. They introduce a set of models where the starch degradation rate is determined by the concentration of T-molecules, which reflect the remaining amount of time (Δt) until the next dawn, together with the concentration of S-molecules, which reflect the total starch content. Their model assumptions lead to the starch degradation rate

$$r = f \cdot \frac{\Delta S^{tot}}{\Delta t} \tag{3}$$

The factor f depends on several structural parameters and kinetic constants. In order to get a complete starch consumption by the time of expected dawn f needs to meet the requirement $f = 1$. The work by Seaton et al. (2014) used three models to explain the control of starch turnover by the circadian clock. All three models involve different interlocked feedback loops, but lead to similar results. The authors conclude that additional experiments are needed to elucidate pathway structure together with an identification of the involved molecular compounds. Seaton et al. (2014) further show how their models provide simple biochemical realizations of the arithmetic division calculation that have been proposed by Scialdone et al. (2013). The modeling approach by Pokhilko et al. (2014) and Pokhilko and Ebenhöh (2015) focuses on the regulation of the carbon metabolism using a circadian timer. The regulation of the C-status is mediated by the kinase SnRK1, while the timing is achieved by the osmotic sensitive kinase OsmK via a circadian regulation of a Ca^{2+}-dependent kinase. Interestingly, in our homeostatic approach the C-status sensing kinase SnRK1 is related to the inflow homeostatic regulation of sucrose (see below).

When testing our model for the behavior shown in Fig. 5a by using different day lengths Φ_L, a linear relationship between k_5 and Φ_L is found (Fig. 5b). This relationship predicts that the primary carbon flux increases proportionally with the day length. This fits very well with many observations that plant growth is generally proportional to the length of the daily exposure to light in the absence of other limiting factors (Garner and Allard, 1920; Romberger, 1963). Fig. 5c shows the model's starch synthesis and degradation behavior for different but constant day lengths. In good agreement with experimental results (Eimert et al., 1995; Gibon et al., 2004; Lu et al., 2005; Zhang et al., 2005), the model shows that for $\Phi_L < 12$ h the rate of starch synthesis is higher during the shorter light period than the rate of starch degradation during the longer dark period. For $\Phi_L > 12$ h the reverse is observed, i.e., the rate of starch synthesis is now lower during the longer light period than the rate of starch degradation during the shorter dark period. When $\Phi_L = 12$ h the rates of starch synthesis and degradation are approximately equal.

Thus, the model predicts that the ability of the plant to measure the amount of received light, i.e., the day length, is crucial for the regulation of its starch utilization. How organisms get information about day length and use it for physiological purposes such as flowering or growth has been a long-standing topic within circadian rhythm research (Bünning, 1973; Taiz et al., 2015).

We have investigated two hypothetical mechanisms for sensing the day length with respect to primary carbon metabolism/growth. The first one is based on two compounds M1 and M2, where M1 is synthesized/activated by light and is a precursor of M2. The conversion from M1 to M2 is suppressed by light and occurs only in darkness, while the deactivation of M2 occurs also in light and at the same rate as M1 is formed. Fig. 6b shows that the sum of M1 and M2 is directly proportional to the length of the light phase Φ_L. Both M1 and M2 activate the primary C-flux by the relationship

$$k_5 = \alpha(M1 + M2) - \beta \tag{4}$$

The parameter α is a scaling factor, while β is related to the light compensation point, i.e., accounting for the required light/photosynthesis which is necessary to maintain respiration at zero growth (arrow in Fig. 5b). The level of M2 is constant during darkness and reflects the total amount of light received during the previous light period. Fig. 6c shows the levels of M1, M2, and their sum when the light dark regime is changed (see arrow) from 8 h:16 h light:dark cycles (short day, SD) to 16 h:8 h (long day, LD) occurring at time $t = 48$ h. M1 increases during the light phase and is converted to M2 in the beginning of the night. During the night M1 is zero, while M2 stays at the maximum level of M1, which has built up during the preceding day. At the beginning of the day M1 increases again while M2 decreases.

Another mechanism based on the homeostatic behavior of a negative feedback loop is shown in Fig. 6d. Here, compound M is generated by light where M induces its own repressor E, which inactivates/removes M. For low $K_M{}^E$ values, M is under a robust homeostatic control (Drengstig et al., 2012a). Under such conditions the steady state level of E reflects the amount of light received, i.e., it is proportional to the day length Φ_L (Fig. 6e). In Fig. 6f we show how the day length sensing mechanism works when going from short days ($\Phi_L = 8$ h) to long days ($\Phi_L = 16$ h). The system needs a certain adaptation time until homeostasis in the average level of M is achieved. The corresponding value of E is a measure for the day length. The time needed for M to reach its set-point is dependent on the magnitudes of the rate constants k_{52} and k_{53}, which also determine the set-point value M_{set}. M_{set} can be found by setting the rate equation of E to zero, i.e., $M_{set} = k_{53}/k_{52} \cdot (E/(K_M^E + E)) \approx k_{53}/k_{52}$, when $K_M^E \ll E$. The adaptation time of the controller can be varied by increasing or decreasing k_{52} and k_{53} while keeping their ratio constant. This generally will lead to a decrease or increase in the adaptation time while M_{set} remains unchanged.

An interesting observation (Lu et al., 2005) is that during the first night after the transition from a short day (SD) to a long day (LD), the starch degradation rate is already increased (Fig. 7a). We have tested the model in this respect, which clearly shows this behavior (Fig. 7b). However, in order to keep the starch content at the end of the dark period adapted to low levels an additional negative feedback together with Michaelis–Menten kinetics is introduced, which in Fig. 1 is outlined in gray. Fig. 7c shows the LD starch adaptation when going from SD ($\Phi_L = 8$ h) to LD ($\Phi_L = 16$ h). The curve from 48 h to 72 h is identical to the one dotted in Fig. 7b.

Fig. 6. Two hypothetical mechanisms to measure day length. Rate equations are given in the Appendix. (a) Mechanism based on light-activation of M1 and its transfer to M2 during the night. (b) The sum of M1 and M2 is proportional to the day length. Rate constants: $k_{40} = 0.05686$, $k_{44} = 1.0 \times 10^3$, $K_I^L = 1.0 \times 10^{-4}$, $K_M^{M2} = 1.0 \times 10^{-6}$. Initial concentrations for M1 and M2 are zero. (c) Time profile of M1 and M2 when L/D cycles are changed from 6 h/18 h to 18 h/6 h, respectively. $M1_0 = 0.0$, $M2_0 = 3.34$. (d) Mechanism for day length measurement based on robust homeostasis of light-induced species M. (e) In the mechanism from panel (d) the average value of controller E is proportional to the day length Φ_L. Rate constant values: $k_{29} = 10.0$ (light phase) or 0.0 (dark phase), $K_a^L = 990$, $k_{51} = 0.00779$, $k_{52} = 0.7$, $k_{53} = 0.07$, $K_M^E = 1.0 \times 10^{-4}$. (f) Transition from short day (SD, $\Phi_L = 8.0$ h) to long day (LD, $\Phi_L = 16.0$ h) conditions at $t = 48$ h (indicated by arrow). $M_0 = 0.075$, $E_0 = 4.277$.

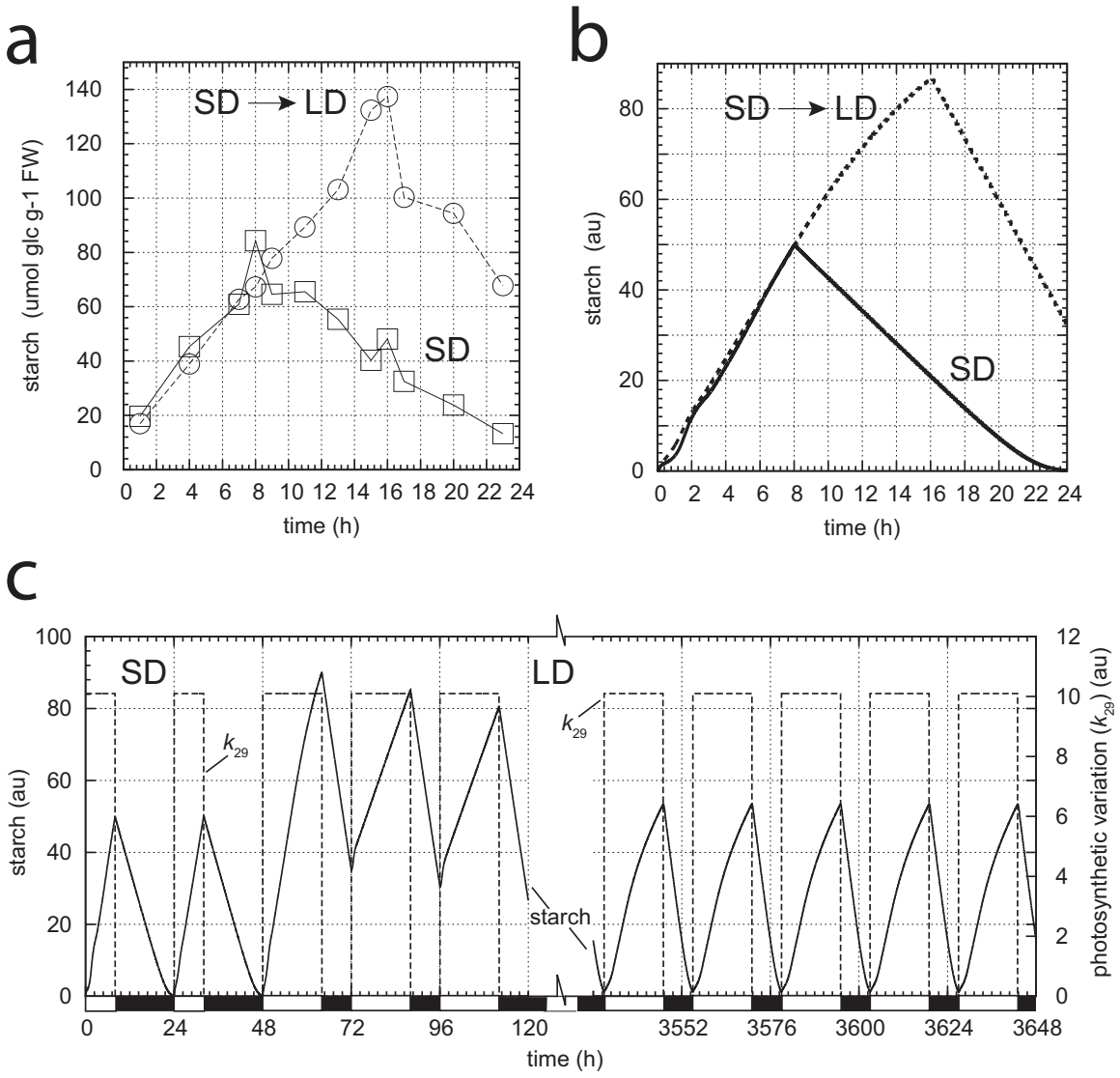

Fig. 7. Starch transition kinetics from short days (SD) to long days (LD). (a) Experimental starch profiles of SD adapted Arabidopsis plants directly after the SD → LD transition (Lu et al., 2005). Panel (b) shows the overlay of the calculated starch profiles (see also panel (c)) between SD-adapted plants (24–48 h) and the first cycle at LD-conditions (48–72 h). (c) Adaptation behavior in starch profile when going from short days (Φ_L=8.0 h) to long days (Φ_L=16.0 h) at t=48 h. The mechanism shown in Fig. 6(a) is used to measure day length Φ_L. To describe the behavior predicted in Fig. 5(b), k_5 is calculated according to the relationship: $k_5 = M1 + M2 - 0.85$. To achieve a stable average starch concentration at different LD phases, the gray outlined parts in Fig. 1 are included using $E_{infl}{}^{TP}$ as an inflow controller with respect to starch. The set-point of this controller is determined by the condition $dE_{infl}^{TP}/dt = 0$, which is given by $(k_{54}/k_{53})\cdot E_{infl}^{TP}/(k_{55} + E_{infl}^{TP}) \approx (k_{54}/k_{53})$. Rate constant values and initial concentrations: $k_1 = 1.0$, $k_2 = 1.0$, $k_3 = 1.0 \times 10^{-5}$, $k_4 = 5.0$, $k_6 = 10.0$, $k_7 = 9.8$, $k_8 = 1.0 \times 10^{-6}$, $k_9 = 1.0$, $k_{10} = 10.0$, $k_{11} = 0.2$, $k_{12} = 15.0$, $k_{13} = 1.0$, $k_{14} = k_{15} = 0.2$, $k_{26} = 0.5$, $k_{27} = 0.1$, $k_{28} = 1.0 \times 10^{-6}$, $k_{29} = 10.1$, $k_{30} = 0.1$, $k_{31} = 2.0$, $k_{32} = 1.0 \times 10^{-6}$, $k_{33} = 1.0 \times 10^{-11}$, $k_{34} = 9.8$, $k_{35} = 10.0$, $k_{36} = 1.0 \times 10^{-4}$, $k_{37} = 0.1$, $k_{38} = 2.0 \times 10^{-2}$, $k_{39} = 1.0 \times 10^{3}$, $k_{40} = 5.68 \times 10^{-2}$, $k_{44} = 1.0 \times 10^{3}$, $K_I^I = 1.0 \times 10^{-4}$, $K_M^{M2} = 1.0 \times 10^{-6}$, $k_{49} = 1.0 \times 10^{-3}$, $k_{53} = 2.5 \times 10^{-4}$, $k_{54} = 6.25 \times 10^{-3}$, $k_{55} = 1.0 \times 10^{-4}$. $\text{sucr}_0 = 5.140 \times 10^{-5}$, $E_{infl,0}^{trioseP} = 6.012$, $E_{outfl,0}^{phe} = 38.677$, $\text{N}_0 = 5.0$, $\text{starch}_0 = 1.046 \times 10^{-7}$, $\text{N}_{ext,0} = 20.0$ (kept constant), $E_{infl,0}^{nitrate} = 18.75$, $\text{trioseP}_0 = 0.0$, $E_{infl,0}^{CO_2} = 2.773$, $E_{infl,0}^{starch} = 55.574$, $\text{M1}_0 = 0.0$, $\text{M2}_0 = 3.342$, and $E_{infl,0}^{TP} = 0.0$.

6. Discussion

The main features of the model are based on the observations that sucrose serves as a hub between primary and secondary metabolite pathways (Wind et al., 2010), that N activates and inhibits primary and secondary metabolism, respectively, and that sucrose levels are under homeostatic control. Sucrose is the major transport form of carbohydrates in higher plants and is also the major osmotic compound in the phloem sap. The apparent constancy of sucrose levels in the phloem sap were first demonstrated by Milburn and coworkers when investigating variable sucrose and potassium exudation rates along with the respective concentrations and fluxes for sucrose and potassium (Smith and Milburn, 1980). By using NMR spectroscopy, the study by Peuke et al. (2001) indicated a diurnal variation of sucrose in 35–45 days old Ricinus plants with an approximately 25% increase in sucrose concentration during the light period. Recently, Kallarackal et al. (2012) reviewed the literature on sucrose homeostasis and by quantifying sap sucrose levels using an enzymatic technique concluded that the sucrose concentrations in young Ricinus plants showed only a marginal diurnal variation. Le Bot et al. (2009) determined the concentrations for several primary and secondary compounds in leaves of young tomato plants as a function of external N concentration, including various sugars and sucrose. The studies by Le Bot et al. showed clearly the up-regulation of secondary metabolites at low N availabilities, while average sucrose levels remained unchanged. Although diurnal variations in sucrose levels cannot be excluded, these studies strongly indicate that sucrose is under a homeostatic regulation.

Homeostasis (Cannon, 1929) involves a combined set of controller motifs, which adjust the inflow and outflow fluxes of the controlled variable in such a way that the concentration of the controlled variable is kept within tolerable limits for the cell/organism (Drengstig et al., 2012a). While homeostasis also includes storage and remobilization of a controlled variable (Huang et al., 2012), we have for the sake of simplicity omitted the vacuolar storage of sucrose and its remobilization from the store (Endler et al., 2006).

The negative feedback loop containing $E_{infl,0}^{trioseP}$ (Fig. 1) is described as an inflow controller motif, which keeps sucrose at a constant level when the demand for sucrose is high, i.e., when sufficient resources are available, the plant is growing and the primary C-flux is high. A molecular component involved in an inflow negative feedback regulation of sucrose is SnRK1 (Sucrose non-fermenting-1-Related protein Kinase), which is activated by sucrose (Tognetti et al., 2013). SnRK1 on its side inactivates Sucrose 6F-phosphatase, an enzyme involved in the synthesis of sucrose. Thus, SnRK1 and sucrose are linked by a negative feedback loop that has an inflow control structure with respect to sucrose (motif 2, Drengstig et al., 2012a). Another important factor which is related in the control of the primary C-flux and plant growth is the kinase TARGET OF RAPAMYCIN (TOR) (Menand et al., 2002). Growth stops when TOR is silenced in Arabidopsis plants by using different RNA interference strategies (Deprost et al., 2007; Dobrenel et al., 2011; Caldana et al., 2013). While these studies indicate that TOR is involved in plant growth and in the regulation of the primary C-flux, the feedback mechanisms from the primary C-compounds regulating TOR are presently not well understood.

The negative feedback including E_{outfl}^{phe} and responsible for the induction of the secondary C-flux, i.e., the upregulation of phenolics under low N conditions, is described as an outflow controller, which moves the accumulating sucrose (due to the decreased primary C-flux at these conditions) into the secondary metabolism. The feedback loop is based on a sucrose-specific induction of PAP1 (Teng et al., 2005; Solfanelli et al., 2006). PAP1 induces TT8, which together with TTG1 and PAP1 activate the phenolic pathway (Baudry et al., 2006; Dubos et al., 2008; Matsui et al., 2008), and thereby consumes sucrose. Interestingly, this sucrose regulating feedback loop contains a positive and a negative feedback loop both regulating the global transcription factors PAP1, TT8 and others (Baudry et al., 2006; Dubos et al., 2008; Matsui et al., 2008). TT8 has been found to be produced in a self-amplifying (autocatalytic) manner (Baudry et al., 2006) and associating in the ternary complex MBW, which includes TT8 and TTG1. MBW activates the synthesis of anthocyanins. Fig. 8a shows a possible scenario of the negative feedback regulation. The autocatalytic formation of TT8 combined with a first-order removal of TT8 provides an effective control (Drengstig et al., 2012b) of PAP1, while the activation of the anthocyanin synthesis by MBW closes the negative feedback regulation of sucrose. The set-point of sucrose for this outflow controller is determined by the rate equation for PAP1. In case k_{65} (which is considered as the Michaelis constant for the PAP1-removing/inactivating enzyme) is low compared to the concentration of PAP1, the sucrose set-point is given by the ratio k_{64}/k_{63} (Drengstig et al., 2012a). The set-point for PAP1 is determined by the rate equation for TT8 and given as the ratio k_{67}/k_{66}. Fig. 8b shows the behavior of the system when the steady state is perturbed by a sudden increase of sucrose at $t=50$ time units. The adaptation of sucrose and PAP1 to their respective set-points is clearly seen and is in qualitative agreement with experimental results (Fig. 6a and b in Solfanelli et al., 2006). Fig. 8c shows a comparison of the system's response behavior with and without an autocatalytic production in TT8. To keep PAP1 still under a homeostatic regulation, rate constant k_{70} (which corresponds to the Michaelis constant of a TT8-removing/inactivating enzyme) has been added. When $k_{70} \ll$ TT8 the set-point for PAP1 is the same as in the autocatalytic case, i.e., $PAP1_{set} = k_{67}/k_{66}$. The response time of the system when TT8 is formed autocatalytically is considerably shorter, while no practical differences in the MBW and TT8 kinetics were observed. The increased effectiveness of PAP1 regulation by autocatalysis may be a reason why a control structure with a positive feedback has developed.

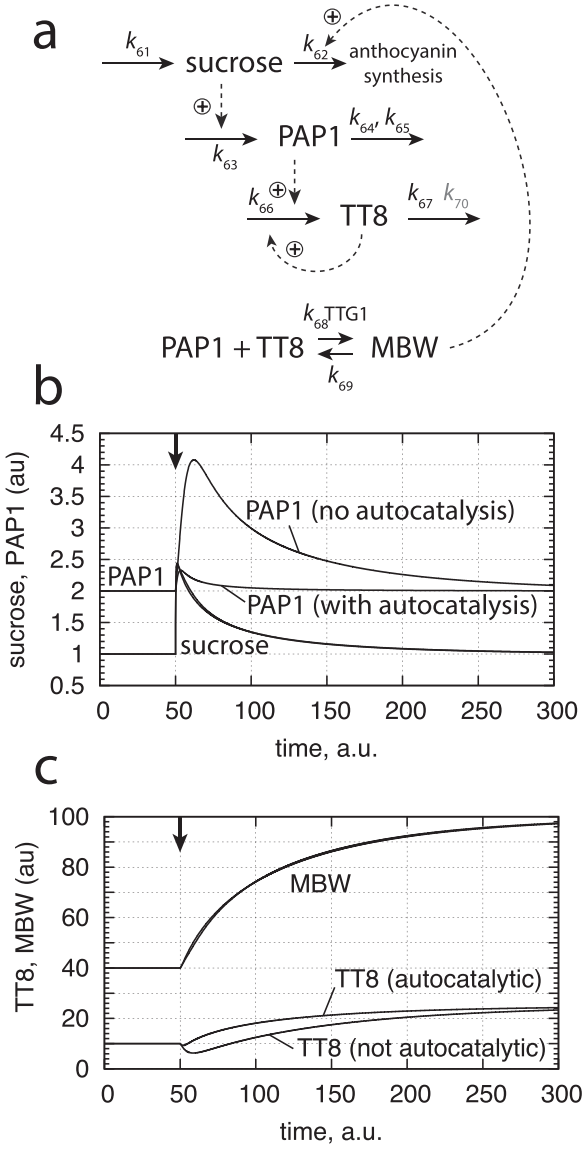

Fig. 8. Comparison of autocatalytic and non-autocatalytic regulation of PAP1 and sucrose. (a) Reaction mechanism. For rate equations see Appendix. (b) At time $t=50$ (arrow) k_{61} is increased from 4.0 to 10.0. PAP1 is regulated more rapidly by the autocatalytic mechanism. Set-points for sucrose and PAP1 are 1.0 and 2.0, respectively. (c) Behavior of the controller molecules MBW and TT8. Rate constants: $k_{62}=0.1$, $k_{63}=k_{64}=1.0$, $k_{65}=1.0\times10^{-4}$, $k_{66}=0.5$, $k_{67}=1.0$, $k_{68}^{TTG1}=2.0$, $k_{69}=1.0$, $k_{70}=1.0\times10^{-4}$. Initial concentrations: sucr $_0=1.0$, PAP1 $_0=2.0$, TT8 $_0=10.0$, MBW $_0=40.0$.

The transcription factor MYBL2 has been identified as a negative regulator of the anthocyanin biosynthesis pathway (Dubos et al., 2008; Matsui et al., 2008). High external sucrose levels down-regulate MYBL2 significantly, while under normal growing conditions the transcript levels of MYBL2 appear unaffected (Nemie-Feyissa et al., 2014). To what extent MYBL2 participates in the switch to secondary metabolism/anthocyanins when N levels are low is presently not known and we have therefore not included MYBL2 in the model.

N has been found to be a global regulator of a variety of processes including activation of photosynthesis, chlorophyll production, primary metabolites (Scheible et al., 2004) and repression of starch metabolism (Scheible et al., 1997). On the other hand, N inhibits the synthesis of phenylalanine (Scheible et al., 2004) as well as the production of anthocyanins by inhibiting the production/activities of PAP1 and PAP2 using the LBD-family of transcription factors (Rubin et al., 2009). These various activation and inhibition processes by N are described in the model by the respective activating and inhibition functions f_{act} and f_I originating from internal N (Fig. 1). N is also a signal contributing to transcriptional regulation of genes coding for key enzymes of the phenylpropanoid pathway (PAL, C4H, 4CL; Fritz et al., 2006).

The typical saw-tooth behavior of starch build-up and consumption is well reflected by the model. During the day, triose-phosphate levels are kept approximately constant such that the rate of starch synthesis under light conditions is approximately constant. During the night, the E_{infl}^{starch} controller maintains sucrose homeostasis and compensates for the (constant) rate of total sucrose consumption by primary and secondary C-fluxes. In this respect, the constant synthesis and degradation rates for starch in the model are closely related to the regulation of triose-phosphate and sucrose homeostasis.

Thus, sucrose homeostasis, regulation of starch content and its adaptation to light–dark regimes, and the diversion of primary C-flux into secondary metabolism are integrated and interconnected mechanisms. The fine-tuned regulation of the allocation of C to secondary metabolism plays a prominent role in plant defense responses under abiotic and biotic constraints and allows to optimize costs of defense.

Acknowledgement

This work was supported in part by a Marie Curie exchange program between the University of Lorraine, France, and the University of Stavanger, Norway and by INRA "Département Environnement et Agronomie" through a grant allowed to P.R.

Appendix A. Rate equations of model

Grayed sections in Fig. 1 are added in the calculations of Fig. 7. Abbreviations: N, internal nitrate; N_{ext}, external nitrate; trioseP, triose phosphate; sucr, sucrose.

$$\frac{d\,sucr}{dt} = k_4 \cdot E_{infl}^{trioseP} \cdot trioseP - k_9 \cdot sucr \cdot E_{outfl}^{phe} \cdot f_I^{phe} - k_5 \cdot sucr \cdot f_{act}^{pcf} - (k_{14} + k_{15}) \cdot sucr + k_{37} \cdot starch \cdot E_{infl}^{starch};$$
$$f_I^{phe} = \frac{k_{38}}{k_{38} + N}; \quad f_{act}^{pcf} = \frac{N}{k_{13} + N} \tag{A.1}$$

$$\frac{d\,E_{infl}^{trioseP}}{dt} = k_1 - \frac{k_2 \cdot sucr \cdot E_{infl}^{trioseP}}{k_3 + E_{infl}^{trioseP}} \tag{A.2}$$

$$\frac{d\,E_{outfl}^{phe}}{dt} = k_6 \cdot sucr \cdot f_I^{E_{outfl}^{phe}} - \frac{k_7 \cdot E_{outfl}^{phe}}{k_8 + E_{outfl}^{phe}}; \quad f_I^{E_{outfl}^{phe}} = \frac{k_{39}}{k_{39} + N} \tag{A.3}$$

$$\frac{d\,N}{dt} = k_{11} \cdot N_{ext} \cdot E_{infl}^{nitrate} - k_{12} \cdot N \tag{A.4}$$

$$\frac{d\,N_{ext}}{dt} = -g \cdot k_{11} \cdot N_{ext} \cdot E_{infl}^{nitrate} \tag{A.5}$$

g: scaling factor due to the size of the external volume

$$\frac{d\,starch}{dt} = k_{10} \cdot trioseP - k_{37} \cdot starch \cdot E_{infl}^{starch} \tag{A.6}$$

$$\frac{d\,E_{infl}^{nitrate}}{dt} = k_{26} - \frac{k_{27} \cdot N \cdot E_{infl}^{nitrate}}{k_{28} + E_{infl}^{nitrate}} \tag{A.7}$$

$$\frac{d\,trioseP}{dt} = k_{29} \cdot f_{act}^{trioseP} \cdot E_{infl}^{CO_2} - \left(k_4 \cdot E_{infl}^{trioseP} + k_{10}\right) \cdot trioseP \tag{A.8}$$

$$f_{act}^{trioseP} = \frac{N}{k_{33} + N}$$
$$\frac{d\,E_{infl}^{CO_2}}{dt} = k_{30} - \frac{k_{31} \cdot trioseP \cdot E_{infl}^{CO_2}}{k_{32} + E_{infl}^{CO_2}} \tag{A.9}$$

$$\frac{d\,E_{infl}^{starch}}{dt} = k_{34} - \frac{k_{35} \cdot sucr \cdot E_{infl}^{starch}}{k_{36} + E_{infl}^{starch}} \tag{A.10}$$

When the adaptation to minimum starch levels at different LD regimes using MM kinetics is included (grayed sections in Fig. 1; results given in Fig. 7) the rate equations for triose-phosphate, starch, and E_{infl}^{TP} change to:

$$\frac{d\,starch}{dt} = \frac{k_{10} \cdot trioseP \cdot f_I}{k_{49} + trioseP} - k_{37} \cdot starch \cdot E_{infl}^{starch} \tag{A.11}$$

$$\text{with } f_I = \frac{k_{56}}{k_{56} + E_{infl}^{TP}}$$
$$\frac{d\,trioseP}{dt} = k_{29} \cdot f_{act}^{trioseP} \cdot E_{infl}^{CO_2} - \left(k_4 \cdot E_{infl}^{trioseP} + \frac{f_I \cdot k_{10}}{k_{49} + trioseP}\right) \cdot trioseP \tag{A.12}$$

$f_{act}^{trioseP}$ and f_I are as described under Eqs. (A.8) and (A.11), respectively.

$$\frac{d\,E_{infl}^{TP}}{dt} = k_{53} \cdot starch - \frac{k_{54} \cdot E_{infl}^{TP}}{k_{55} + E_{infl}^{TP}} \tag{A.13}$$

Appendix B. Rate equations for daylength measuring mechanism in Fig. 6a

$$\frac{d\,M1}{dt} = k_{29} \cdot k_{40} - \frac{k_{44} \cdot K_I^L \cdot M1}{K_I^L + k_{29}} \tag{B.1}$$

$$\frac{d\,M2}{dt} = \frac{k_{44} \cdot K_I^L \cdot M1}{K_I^L + k_{29}} - \frac{k_{29} \cdot k_{40} \cdot M2}{K_M^{M2} + M2} \tag{B.2}$$

Appendix C. Rate equations for daylength measuring mechanism in Fig. 6d

$$\frac{d\,M}{dt} = k_{50} - k_{51} \cdot M \cdot E; \quad \text{with } k_{50} = f_{act}^{M} = \frac{k_{29}}{K_a^L + k_{29}} \tag{C.1}$$

$$\frac{d\,E}{dt} = k_{52}\cdot M - \frac{k_{53}\cdot E}{K_M^E + E} \tag{C.2}$$

Appendix D. Rate equations for sucrose and PAP1 regulation by TT8/MBW (Fig. 8a)

$$\frac{d\,sucr}{dt} = k_{61} - k_{62}\cdot sucr\cdot MBW \tag{D.1}$$

$$\frac{d\,PAP1}{dt} = k_{63}\cdot sucr - \frac{k_{64}PAP1}{k_{65} + PAP1} - k_{68}^{TTG1}\cdot PAP1\cdot TT8 + k_{69}\cdot MBW \tag{D.2}$$

$$\frac{d\,MBW}{dt} = k_{68}^{TTG1}\cdot PAP1\cdot TT8 - k_{69}\cdot MBW \tag{D.3}$$

Non-autocatalytic regulation of PAP1:

$$\frac{d\,TT8}{dt} = k_{66}\cdot PAP1 - \frac{k_{67}\cdot TT8}{k_{70} + TT8} - k_{68}^{TTG1}\cdot PAP1\cdot TT8 + k_{69}\cdot MBW \tag{D.4}$$

Autocatalytic regulation of PAP1:

$$\frac{d\,TT8}{dt} = k_{66}\cdot PAP1\cdot TT8 - k_{67}\cdot TT8 - k_{68}^{TTG1}\cdot PAP1\cdot TT8 + k_{69}\cdot MBW \tag{D.5}$$

References

Abro, M.A., Lecompte, F., Bryone, F., Nicot, P.C., 2013. Nitrogen fertilization of the host plant influences production and pathogenicity of *Botrytis cinerea* secondary inoculum. Phytopathology 103 (3), 261–267.

Baudry, A., Caboche, M., Lepiniec, L., 2006. TT8 controls its own expression in a feedback regulation involving TTG1 and homologous MYB and bHLH factors, allowing a strong and cell-specific accumulation of flavonoids in *Arabidopsis thaliana*. Plant J. 46 (5), 768–779.

Bryant, J.P., Chapin III, F.S., Klein, D.R., 1983. Carbon/nutrient balance of boreal plants in relation to vertebrate herbivory. Oikos, 357–368.

Bünning, E., 1973. The Physiological Clock, Circadian Rhythms and Biological Chronometry. Springer-Verlag, Berlin.

Caldana, C., Li, Y., Leisse, A., Zhang, Y., Bartholomaeus, L., Fernie, A.R., Willmitzer, L., Giavalisco, P., 2013. Systemic analysis of inducible target of rapamycin mutants reveal a general metabolic switch controlling growth in *Arabidopsis thaliana*. Plant J. 73 (6), 897–909.

Cannon, W., 1929. Organization for physiological homeostasis. Physiol. Rev. 9, 399–431.

Deprost, D., Yao, L., Sormani, R., Moreau, M., Leterreux, G., Nicolaï, M., Bedu, M., Robaglia, C., Meyer, C., 2007. The Arabidopsis TOR kinase links plant growth, yield, stress resistance and mRNA translation. EMBO Rep. 8 (9), 864–870.

Dijkwel, P.P., Kock, P.A., Bezemer, R., Weisbeek, P.J., Smeekens, S.C., 1996. Sucrose represses the developmentally controlled transient activation of the plastocyanin gene in *Arabidopsis thaliana* seedlings. Plant Physiol. 110 (2), 455–463.

Dobrenel, T., Marchive, C., Sormani, R., Moreau, M., Mozzo, M., Montané, M.-H., Menand, B., Robaglia, C., Meyer, C., 2011. Regulation of plant growth and metabolism by the TOR kinase. Biochem. Soc. Trans. 39 (2), 477–481.

Doré, T., Makowski, D., Malézieux, E., Munier-Jolain, N., Tchamitchian, M., Tittonell, P., 2011. Facing up to the paradigm of ecological intensification in agronomy: revisiting methods, concepts and knowledge. Eur. J. Agron. 34 (4), 197–210.

Drengstig, T., Jolma, I., Ni, X., Thorsen, K., Xu, X., Ruoff, P., 2012a. A basic set of homeostatic controller motifs. Biophys. J. 103 (9), 2000–2010.

Drengstig, T., Ni, X., Thorsen, K., Jolma, I., Ruoff, P., 2012b. Robust adaptation and homeostasis by autocatalysis. J. Phys. Chem. B 116 (18), 5355–5363.

Dubos, C., Le Gourrierec, J., Baudry, A., Huep, G., Lanet, E., Debeaujon, I., Routaboul, J.-M., Alboresi, A., Weisshaar, B., Lepiniec, L., 2008. MYBL2 is a new regulator of flavonoid biosynthesis in Arabidopsis thaliana. Plant J. 55 (6), 940–953.

Eimert, K., Wang, S.-M., Lue, W., Chen, J., 1995. Monogenic recessive mutations causing both late floral initiation and excess starch accumulation in arabidopsis. Plant Cell 7 (10), 1703–1712.

Endler, A., Meyer, S., Schelbert, S., Schneider, T., Weschke, W., Peters, S.W., Keller, F., Baginsky, S., Martinoia, E., Schmidt, U.G., 2006. Identification of a vacuolar sucrose transporter in barley and arabidopsis mesophyll cells by a tonoplast proteomic approach. Plant Physiol. 141 (1), 196–207.

Farquhar, G., von Caemmerer, S.v., Berry, J., 1980. A biochemical model of photosynthetic CO_2 assimilation in leaves of C_3 species. Planta 149 (1), 78–90.

Feugier, F.G., Satake, A., 2013. Dynamical feedback between circadian clock and sucrose availability explains adaptive response of starch metabolism to various photoperiods. Front. Plant Sci. 3 (305). http://dx.doi.org/10.3389/fpls.2012.00305.

Fritz, C., Palacios-Rojas, N., Feil, R., Stitt, M., 2006. Regulation of secondary metabolism by the carbon-nitrogen status in tobacco: nitrate inhibits large sectors of phenylpropanoid metabolism. Plant J. 46 (4), 533–548.

Garner, W.W., Allard, H.A., 1920. Effect of the relative length of day and night and other factors of the environment on growth and reproduction in plants. J. Agric. Res. 18, 553–606.

Geiger, M., Haake, V., Ludewig, F., Sonnewald, U., Stitt, M., 1999. The nitrate and ammonium nitrate supply have a major influence on the response of photosynthesis, carbon metabolism, nitrogen metabolism and growth to elevated carbon dioxide in tobacco. Plant Cell Environ. 22 (10), 1177–1199.

Gibon, Y., Bläsing, O.E., Palacios-Rojas, N., Pankovic, D., Hendriks, J.H., Fisahn, J., Höhne, M., Günther, M., Stitt, M., 2004. Adjustment of diurnal starch turnover to short days: depletion of sugar during the night leads to a temporary inhibition of carbohydrate utilization, accumulation of sugars and post-translational activation of ADP-glucose pyrophosphorylase in the following light period. Plant J. 39 (6), 847–862.

Glynn, C., Herms, D.A., Orians, C.M., Hansen, R.C., Larsson, S., 2007. Testing the growth-differentiation balance hypothesis: dynamic responses of willows to nutrient availability. New Phytol. 176 (3), 623–634.

Hanson, J., Hanssen, M., Wiese, A., Hendriks, M.M., Smeekens, S., 2008. The sucrose regulated transcription factor bZIP11 affects amino acid metabolism by regulating the expression of ASPARAGINE SYNTHETASE1 and PROLINE DEHYDROGENASE2. Plant J. 53 (6), 935–949.

Herms, D.A., Mattson, W.J., 1992. The dilemma of plants: to grow or defend. Q. Rev. Biol. 67 (3), 283–335.

Huang, Y., Drengstig, T., Ruoff, P., 2012. Integrating fluctuating nitrate uptake and assimilation to robust homeostasis. Plant Cell Environ. 35, 917–928.

Huber, S., Huber, J., McMichael, R., 1992. The regulation of sucrose synthesis in leaves. In: Pollock, C., Farrar, J., Gordon, A. (Eds.), Carbon Partitioning: Within and Between Organisms. Bios Scientific Publishers, Oxford, pp. 1–26.

Kallarackal, J., Bauer, S.N., Nowak, H., Hajirezaei, M.-R., Komor, E., 2012. Diurnal changes in assimilate concentrations and fluxes in the phloem of castor bean (*Ricinus communis* L.) and tansy (*Tanacetum vulgare* L.). Planta 236 (1), 209–223.

Kingston-Smith, A.H., Bollard, A.L., Minchin, F.R, 2005. Stress-induced changes in protease composition are determined by nitrogen supply in non-nodulating white clover. J. Exp. Bot. 56 (412), 745–753.

Koricheva, J., Larsson, S., Haukioja, E., Keinänen, M., 1998. Regulation of woody plant secondary metabolism by resource availability: hypothesis testing by means of meta-analysis. Oikos, 212–226.

Larbat, R., Le Bot, J., Bourgaud, F., Robin, C., Adamowicz, S., 2012. Organ-specific responses of tomato growth and phenolic metabolism to nitrate limitation. Plant Biol. 14 (5), 760–769.

Le Bot, J., Bénard, C., Robin, C., Bourgaud, F., Adamowicz, S., 2009. The 'trade-off' between synthesis of primary and secondary compounds in young tomato leaves is altered by nitrate nutrition: experimental evidence and model consistency. J. Exp. Bot. 60, 4301–4314.

Lillo, C., Lea, U.S., Ruoff, P., 2008. Nutrient depletion as a key factor for manipulating gene expression and product formation in different branches of the flavonoid pathway. Plant Cell Environ. 31 (5), 587–601.

Loomis, W., 1932. Growth-differentiation balance vs. carbohydrate-nitrogen ratio. Proc. Am. Soc. Hortic. Sci. 29, 240–245.

Lu, Y., Gehan, J.P., Sharkey, T.D., 2005. Daylength and circadian effects on starch degradation and maltose metabolism. Plant Physiol. 138 (4), 2280–2291.

Marschner, P., 2012. Marschner's Mineral Nutrition of Higher Plants, 3rd edition. Academic Press, Amsterdam.

Massad, T.J., Dyer, L.A., Vega, G., 2012. Costs of defense and a test of the carbon-nutrient balance and growth-differentiation balance hypotheses for two co-occurring classes of plant defense. PLOS One 7 (10), e47554.

Matsui, K., Umemura, Y., Ohme-Takagi, M., 2008. Atmybl2, a protein with a single myb domain, acts as a negative regulator of anthocyanin biosynthesis in arabidopsis. Plant J. 55 (6), 954–967.

McKey, D., 1974. Adaptive patterns in alkaloid physiology. Am. Nat., 305–320.

Menand, B., Desnos, T., Nussaume, L., Berger, F., Bouchez, D., Meyer, C., Robaglia, C., 2002. Expression and disruption of the arabidopsis TOR (Target Of Rapamycin) gene. Proc. Natl. Acad. Sci. USA 99 (9), 6422–6427.

Miller, A.J., Smith, S.J., 1992. The mechanism of nitrate transport across the tonoplast of barley root cells. Planta 187 (4), 554–557.

Miller, A.J., Smith, S.J., 2008. Cytosolic nitrate ion homeostasis: could it have a role in sensing nitrogen status?. Ann. Bot. 101 (4), 485–489.

Mooney, K.A., Halitschke, R., Kessler, A., Agrawal, A.A., 2010. Evolutionary trade-offs in plants mediate the strength of trophic cascades. Science 327 (5973), 1642–1644.

Nemie-Feyissa, D., Olafsdottir, S.M., Heidari, B., Lillo, C., 2014. Nitrogen depletion and small R3-MYB transcription factors affecting anthocyanin accumulation in arabidopsis leaves. Phytochemistry 98, 34–40.

Nguyen, P.M., Niemeyer, E.D., 2008. Effects of nitrogen fertilization on the phenolic composition and antioxidant properties of basil (*Ocimum basilicum* L.). J. Agric. Food Chem. 56 (18), 8685–8691.

Ni, X., Drengstig, T., Ruoff, P., 2009. The control of the controller: molecular mechanisms for robust perfect adaptation and temperature compensation. Biophys. J. 97, 1244–1253.

Peuke, A., Rokitta, M., Zimmermann, U., Schreiber, L., Haase, A., 2001. Simultaneous measurement of water flow velocity and solute transport in xylem and phloem

of adult plants of ricinus communis over a daily time course by nuclear magnetic resonance spectrometry. Plant Cell Environ. 24 (5), 491–503.
Pokhilko, A., Ebenhöh, O., 2015. Mathematical modelling of diurnal regulation of carbohydrate allocation by osmo-related processes in plants. J. R. Soc. Interface 12 (104), 20141357.
Pokhilko, A., Flis, A., Sulpice, R., Stitt, M., Ebenhöh, O., 2014. Adjustment of carbon fluxes to light conditions regulates the daily turnover of starch in plants: a computational model. Mol. BioSyst. 10 (3), 613–627.
Pretorius, J., Nieuwoudt, D., Eksteen, D., 1999. Sucrose synthesis and translocation in *Zea mays* L. during early growth, when subjected to N and K deficiency. S. Afr. J. Plant Soil 16 (4), 173–179.
Radhakrishnan, K., Hindmarsh, A., 1993. Description and Use of LSODE, the Livermore Solver for Ordinary Differential Equations. NASA Reference Publication 1327, Lawrence Livermore National Laboratory Report UCRL-ID-113855. National Aeronautics and Space Administration, Lewis Research Center, Cleveland, OH 44135-3191.
Romberger, J.A., 1963. Meristems, Growth, and Development in Woody Plants: An Analytical Review of Anatomical, Physiological, and Morphogenic Aspects. No. 1293. US Government Printing Office.
Royer, M., Larbat, R., Le Bot, J., Adamowicz, S., Robin, C., 2013. Is the C:N ratio a reliable indicator of C allocation to primary and defence-related metabolisms in tomato? Phytochemistry 88, 25–33.
Rubin, G., Tohge, T., Matsuda, F., Saito, K., Scheible, W.-R., 2009. Members of the LBD family of transcription factors repress anthocyanin synthesis and affect additional nitrogen responses in Arabidopsis. Plant Cell 21 (11), 3567–3584.
Scheible, W.-R., Lauerer, M., Schulze, E.-D., Caboche, M., Stitt, M., 1997. Accumulation of nitrate in the shoot acts as a signal to regulate shoot-root allocation in tobacco. Plant J. 11 (4), 671–691.
Scheible, W.-R., Morcuende, R., Czechowski, T., Fritz, C., Osuna, D., Palacios-Rojas, N., Schindelasch, D., Thimm, O., Udvardi, M.K., Stitt, M., 2004. Genome-wide reprogramming of primary and secondary metabolism, protein synthesis, cellular growth processes, and the regulatory infrastructure of Arabidopsis in response to nitrogen. Plant Physiol. 136 (1), 2483–2499.
Scialdone, A., Howard, M., 2015. How plants manage food reserves at night: quantitative models and open questions. Front. Plant Sci. 6, 204.
Scialdone, A., Mugford, S.T., Feike, D., Skeffington, A., Borrill, P., Graf, A., Smith, A.M., Howard, M., 2013. Arabidopsis plants perform arithmetic division to prevent starvation at night. Elife 2, e00669.
Seaton, D.D., Ebenhöh, O., Millar, A.J., Pokhilko, A., 2014. Regulatory principles and experimental approaches to the circadian control of starch turnover. J. R. Soc. Interface 11 (91), 20130979.
Smith, A.M., Stitt, M., 2007. Coordination of carbon supply and plant growth. Plant Cell Environ. 30 (9), 1126–1149.
Smith, J.A.C., Milburn, J.A., 1980. Phloem transport, solute flux and the kinetics of sap exudation in *Ricinus communis* L. Planta 148 (1), 35–41.
Solfanelli, C., Poggi, A., Loreti, E., Alpi, A., Perata, P., 2006. Sucrose-specific induction of the anthocyanin biosynthetic pathway in arabidopsis. Plant Physiol. 140 (2), 637–646.
Stamp, N., 2003. Out of the quagmire of plant defense hypotheses. Q. Rev. Biol. 78 (1), 23–55.
Stamp, N., 2004. Can the growth-differentiation balance hypothesis be tested rigorously? Oikos 107 (2), 439–448.
Stewart, A., Chapman, W., Jenkins, G., Graham, I., Martin, T., Crozier, A., 2001. The effect of nitrogen and phosphorus deficiency on flavonol accumulation in plant tissues. Plant Cell Environ. 24 (11), 1189–1197.
Stitt, M., Zeeman, S.C., 2012. Starch turnover: pathways, regulation and role in growth. Curr. Opin. Plant Biol. 15 (3), 282–292.
Taiz, L., Zeiger, E., Møller, I.M., Murphy, A.S., 2015. Plant Physiology and Development. Sinauer, Sunderland.
Teng, S., Keurentjes, J., Bentsink, L., Koornneef, M., Smeekens, S., 2005. Sucrose-specific induction of anthocyanin biosynthesis in arabidopsis requires the MYB75/PAP1 gene. Plant Physiol. 139 (4), 1840–1852.
Thorsen, K., Drengstig, T., Ruoff, P., 2013. Control theoretic properties of physiological controller motifs. In: ICSSE 2013, IEEE International Conference on System Science and Engineering. Budapest, pp. 165–170.
Tognetti, J.A., Horacio, P., Martinez-Noel, G., 2013. Sucrose signaling in plants: a world yet to be explored. Plant Signal. Behav. 8 (3), e23316.
Vidal, E.A., Gutierrez, R.A., 2008. A systems view of nitrogen nutrient and metabolite responses in Arabidopsis. Curr. Opin. Plant Biol. 11 (5), 521–529.
Von Caemmerer, S., Farquhar, G., 1981. Some relationships between the biochemistry of photosynthesis and the gas exchange of leaves. Planta 153 (4), 376–387.
Wilkie, J., Johnson, M., Reza, K., 2002. Control Engineering. An Introductory Course. Palgrave, New York.
Wind, J., Smeekens, S., Hanson, J., 2010. Sucrose: metabolite and signaling molecule. Phytochemistry 71 (14), 1610–1614.
Xu, G., Fan, X., Miller, A.J., 2012. Plant nitrogen assimilation and use efficiency. Annu. Rev. Plant Biol. 63, 153–182.
Yi, T., Huang, Y., Simon, M., Doyle, J., 2000. Robust perfect adaptation in bacterial chemotaxis through integral feedback control. Proc. Natl. Acad. Sci. USA 97 (9), 4649–4653.
Zhang, X., Myers, A.M., James, M.G., 2005. Mutations affecting starch synthase III in arabidopsis alter leaf starch structure and increase the rate of starch synthesis. Plant Physiol. 138 (2), 663–674.
Züst, T., Joseph, B., Shimizu, K.K., Kliebenstein, D.J., Turnbull, L.A., 2011. Using knockout mutants to reveal the growth costs of defensive traits. Proc. R. Soc. Lond. B: Biol. Sci., http://dx.doi.org/10.1098/rspb.2010.2475.